Materials Transactions, Vol. 43, No. 8 (2002) pp. 1833 to 1839
Special Issue on Lead-Free Electronics Packaging

Melting and Joining Behavior of Sn/Ag and Sn–Ag/Sn–Bi Plating on Cu Core Ball

Keisuke Uenishi[1], Yasuhiro Kohara[1, *1], Shigeaki Sakatani[1,*1], Toshio Saeki[1, *2], Kojiro F. Kobayashi[1] and Masaharu Yamamoto[2]

[1]*Department of Manufacturing Science, Graduate School of Engineering, Osaka University, Suita 565-0871, Japan*
[2]*Kagoshima Sumitoku Electronics Co., Ltd., Izumi 899-0201, Japan*

We fabricated Cu core Sn–Ag solder balls by plating pure Sn and Ag on Cu balls and clarified that Sn/Ag plating began to melt at a rather low temperature, the eutectic temperature of Sn–Ag–Cu. This early melting at the eutectic temperature was ascribed to the diffusion of Cu and Ag into the Sn plating during the heating process. We investigated the solderability of the BGA joint with the Ni/Au coated Cu pad to compare it with that of the commercial Sn–Ag and Sn–Ag–Cu balls. After reflow soldering, we observed a eutectic microstructure composed of β-Sn, Ag_3Sn, and Cu_6Sn_5 phases in the solder, and a η'-$(Au, Cu, Ni)_6Sn_5$ reaction layer was formed at the interface between the solder and the Cu pad. The BGA joint using Cu core solder balls could prevent the degradation of joint strength during aging at 423 K because of the slower growth rate of the η'-$(Au, Cu, Ni)_6Sn_5$ reaction layer formed at the solder-pad interface. Furthermore, we were able to fabricate Cu-cored, multicomponent Sn–Ag–Bi balls by sequentially coating binary Sn–Ag and Sn–Bi solders onto Cu balls. The coated balls also exhibited almost the same melting and soldering behaviors as those of the previously alloyed Sn–2Ag–0.75Cu–3Bi solders.

(Received March 11, 2002; Accepted July 2, 2002)

Keywords: *ball grid array, lead free solder, intermetallic compound, copper cored ball, reaction layer, shear strength*

1. Introduction

Ball grid array (BGA) packages have advantages over more conventional packages, such as the pin through-hole or quad flat packages, including higher input-output terminal density, smaller footprint, and higher reliability.[1)] In the BGA packaging, module chips and substrates are usually connected by solder balls. Employing Cu-cored solder balls in BGA packaging improves thermal and electrical performance over monolithic solder balls due to their Cu cores. Besides, Cu-core balls have higher stiffness for maintaining the distance between chips and substrates.[2)] Thus, BGA packaging using Cu-core balls is a candidate solution for high-power, high-performance applications.

The authors previously reported that Cu-core Sn–Pb solder balls can effectively control the interaction of solders with both Au/Ni electroplated[3,4)] and electroless-plated Cu pads.[5,6)] Specifically, Cu that dissolves from the core ball into the solder during reflow forms a Cu–Sn based reaction layer at the interface between the solder ball and pad.[7,8)] Since most of this dissolved Cu was consumed to form the Cu–Sn reaction layer and little Cu is left in the solder ball, this Cu–Sn based reaction layer grows very little during thermal exposure at 423 K. Consequently, the joint strength using Cu core balls is only slightly degraded by thermal exposure at 423 K.

Recent environmental regulations against using Sn–Pb solder require the development of substantially Pb-free solders. Development of Cu-cored, Pb-free solder balls is thus an urgent issue. In particular, the effect of Cu-core balls on controlling the interaction with Au/Ni plating will be a key issue in obtaining reliable BGA joints since this interaction is reported to be enhanced for Pb-free solders due to its higher reflow temperature and larger molar fraction of Sn.[9–11)]

Cu-core Sn–Pb solder balls are normally prepared by electroplating solder on Cu balls. After the promotion of research to develop Pb-free solders, Sn–Ag based solders were recognized as the most promising candidates due to their superior mechanical properties. At this moment, however, techniques for plating Sn–Ag solders onto the desired composition have not been established.

Thus, the authors fabricated Cu-cored Sn–Ag solder balls by plating pure Sn and Ag onto Cu balls. Using such balls in BGA packages will be very advantageous because it will be easier to control plating conditions and the composition of solder by changing the plating thicknesses. In order to extend this technique to multicomponent solders, we fabricated Cu-core Sn–Ag–Bi balls by sequentially plating binary Sn–Bi and Sn–Ag solders onto Cu balls.

The present research investigated the melting behavior of the Sn/Ag or Sn–Bi/Sn–Ag (SB/SA) plating by differential scanning calorimetry. The solderability of the BGA joint with the Ni- or Au-coated Cu pad was also evaluated by observing the microstructure and performing joint shear tests for both the reflowed and thermally exposed joints.

Obtained results were compared with those using the previously alloyed commercial Sn–Ag, Sn–Ag–Cu and Sn–Ag–Cu–Bi balls.

2. Experimental Procedure

The BGA substrates used in this experiment are 7 μm thick Ni and 1.5 μm thick Au electroplated or electroless-plated Cu pads. The electroplated (electroless-plated) Ni coating contained Co (P) as a contaminant.

We fabricated Cu-cored Sn–Ag solder balls by sequentially coating pure Sn and Ag onto Cu balls and Cu-cored Sn–Ag–Bi balls by coating binary Sn–3.5 mass%Ag and Sn–

*1Graduate Student, Osaka University.
*2Graduate Student, Osaka University, Present address: Hitachi Co. Ltd., Yokohama 244-8567, Japan.

Table 1 Thickness of the each layer plated on Cu core balls.

Solder balls	Plate	Thickness (μm)
Sn/Ag Cu core ball	Sn	34.2
	Ag	0.8
SB/SA Cu core ball	Sn–7Bi	15.8
	Sn–3.5Ag	19.2

7 mass%Bi solders onto Cu balls. Table 1 presents the thickness of each plating. In this condition, the total composition of plating coated onto Cu-core balls is designed to be Sn–3.5 mass%Ag and Sn–2 mass%Ag–3 mass%Bi. Thickness variations in each plating change the composition, and the difference from the desired composition was controlled to be less than 0.4 mass% in this experiment.

Previously alloyed commercial Sn–3.5 mass%Ag, Sn–3.5 mass%Ag–0.76 mass%Cu and Sn–2 mass%Ag–0.75 mass%Cu–3 mass%Bi solder balls were also prepared as references. Ball diameters were fixed to 740 μm. Figure 1 schematically illustrates the solder ball and pad for the BGA joint used in this study. The melting behavior of the solder balls was investigated by differential scanning calorimetry (DSC, Perkin-Elmer DSC7) at various heating rates. For the BGA joining, solder balls were dipped into rosin flux and then planted on the pads manually. The solder balls were reflowed by using a hot air oven. The peak reflow temperature was 518 K and reflow time for the solder balls to melt was 90 s. After reflowing the solder, we subjected the BGA joints to additional heat exposure at an aging temperature of 423 K for 0.5 h to 500 h. To investigate the microstructure evolution of the joints, we observed the cross sections of the samples by scanning electron microscopy (SEM) with energy depressive X-ray (EDX) analyses. We prepared samples for transmission electron microscopy (TEM) observation by using a focused-ion-beam milling apparatus and measured the strength of the obtained BGA joints through the shear fracture test. The shear tool was set 0.1 mm distant from the substrate and the traverse speed was fixed to 0.2 mm/s.

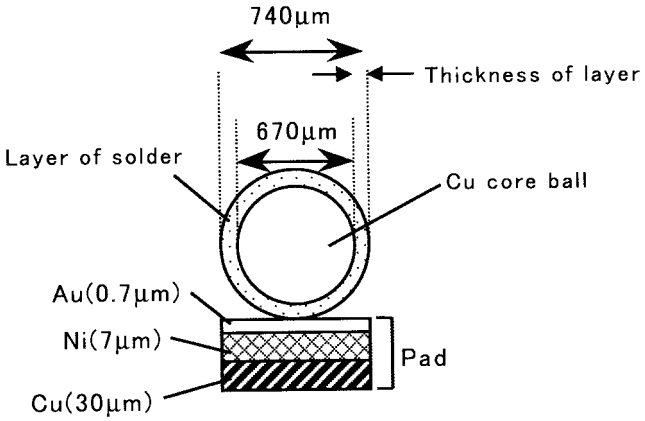

Fig. 1 Schematic illustration of solder ball and pad for BGA joints used in this study.

3. Results and Discussion

3.1 Microstructure of as plated solder balls

Figure 2 depicts the microstructure of the plated solder balls. All of the layers were densely plated to the desired thickness on Cu-core balls, and no defects could be observed at the interface between each plating or between the plating and Cu balls. Diffusion of elements was not detected in Sn and Ag platings for the Sn/Ag-plated Cu-core balls. For the SB/SA balls, Sn–Ag plating exhibited an Sn-based microstructure with dispersed Ag_3Sn particles, while a single-phase Sn solid containing Bi was observed in Sn–Bi plating. Moreover, approximately 1.8 mol%Bi was detected in Sn–Ag plating by EDX analysis, showing the diffusion of Bi from Sn–Bi to Sn–Ag plating. The diffusivity of Bi in Sn is reported to be about $D = 1.93 \times 10^{-10}$ mm^2/s at 298 K,[12] so the diffusion distance, $(Dt)^{1/2}$, of Bi reaches about 4 μm during holding even at room temperature for 10 days. Moreover, holding at 350 K during plating supposedly enhances diffusion.

3.2 Melting behavior of solder balls

Figure 3 presents DSC curves of the various solders during continuous heating at a rate of 1 K/s. As shown, Sn/Ag-plated Cu-core balls exhibited melting behavior similar to Sn–Ag–Cu solder balls, not to Sn–Ag solder. Even changing the heating rate, as shown in Fig. 4, produces significant differences

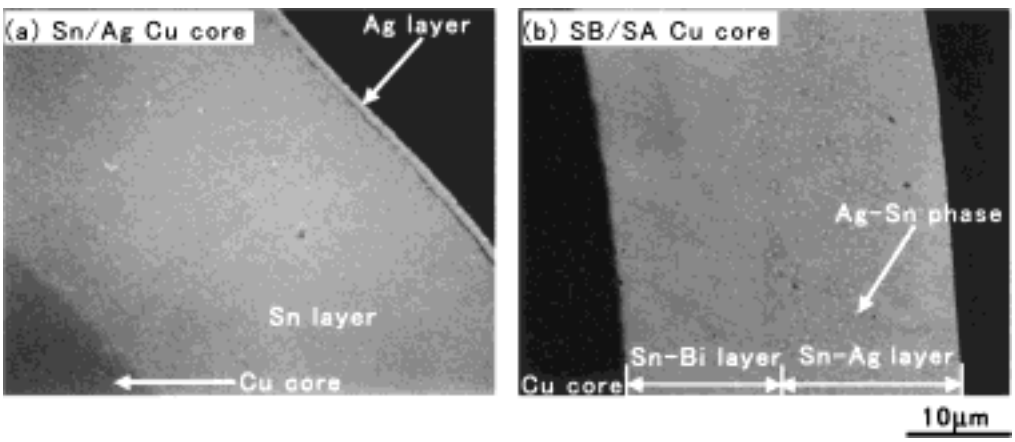

Fig. 2 SEM images of the microstructure for as plated (a) Sn/Ag and (b) SB/SA solder balls with Cu core.

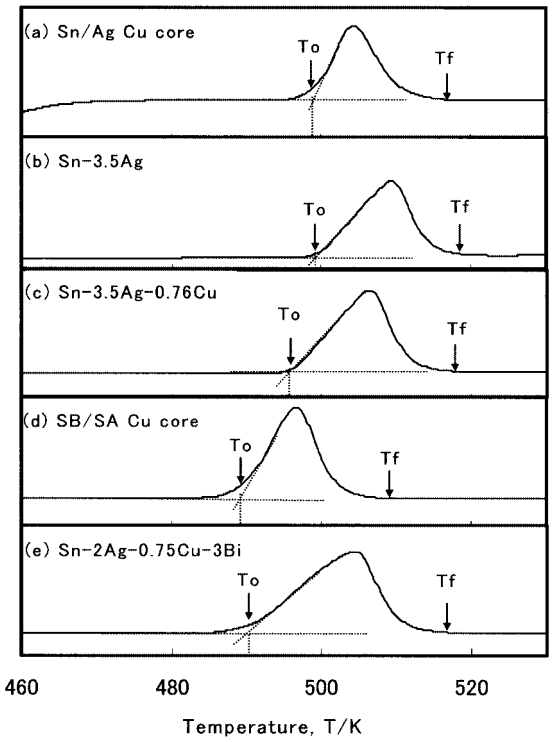

Fig. 3 DSC curves of (a) Sn/Ag Cu core, (b) Sn–Ag–Cu, (c) SB/SA Cu core and (d) Sn–Ag–Cu–Bi solder balls at a rate of 1 K/s.

Table 2 Measured onset temperature (*To*) and offset temperature (*Tf*) for various solder balls. To was obtained by extrapolating the value at a heating rate of 0 K/s. *Tf* is the value measured at a heating rate of 1 K/s.

Solder balls	*To* (K)	*Tf* (K)
Sn/Ag Cu core ball	489	519
SB/SA Cu core ball	483	513
Sn–3.5Ag	494	525
Sn–3.5Ag–0.76Cu	489	519
Sn–2Ag–0.75Cu–3Bi	481	517

for the onset and offset of melting between Sn/Ag-plated Cu balls and Sn–Ag–Cu solder balls.[13,14] In addition, SB/SA balls melted like Sn–Ag–Cu–Bi balls.[15] There was a rather linear relationship between the heating rate and onset temperature for all of the solders. Since the onset melting temperature is dependent on the heating rate, the solidus temperature is generally determined as the value at the heating rate of 0 K/s by extrapolating this relation. Table 2 shows the determined onset temperature. To, for various solder balls. Due to the Bi in solder, the onset temperature decreased to about 483 K. In order to investigate the why Sn/Ag or SB/SA balls exhibit such melting behavior, we observed the microstructure and performed EDX analyses for the balls heated to just below the onset melting temperature. Quantitative EDX analysis for Sn and Ag plating confirmed that 0.3 mass% of Cu diffused into Sn plating. Furthermore, η'-Cu_6Sn_5 (Ag_3Sn) reaction layers were formed at the interface of Sn plating with Cu ball (Ag) plating. When the Cu-core solder balls were heated, Cu, Ag and Bi diffused into Sn, making the composition of Sn nearly ternary or quarterly eutectic.

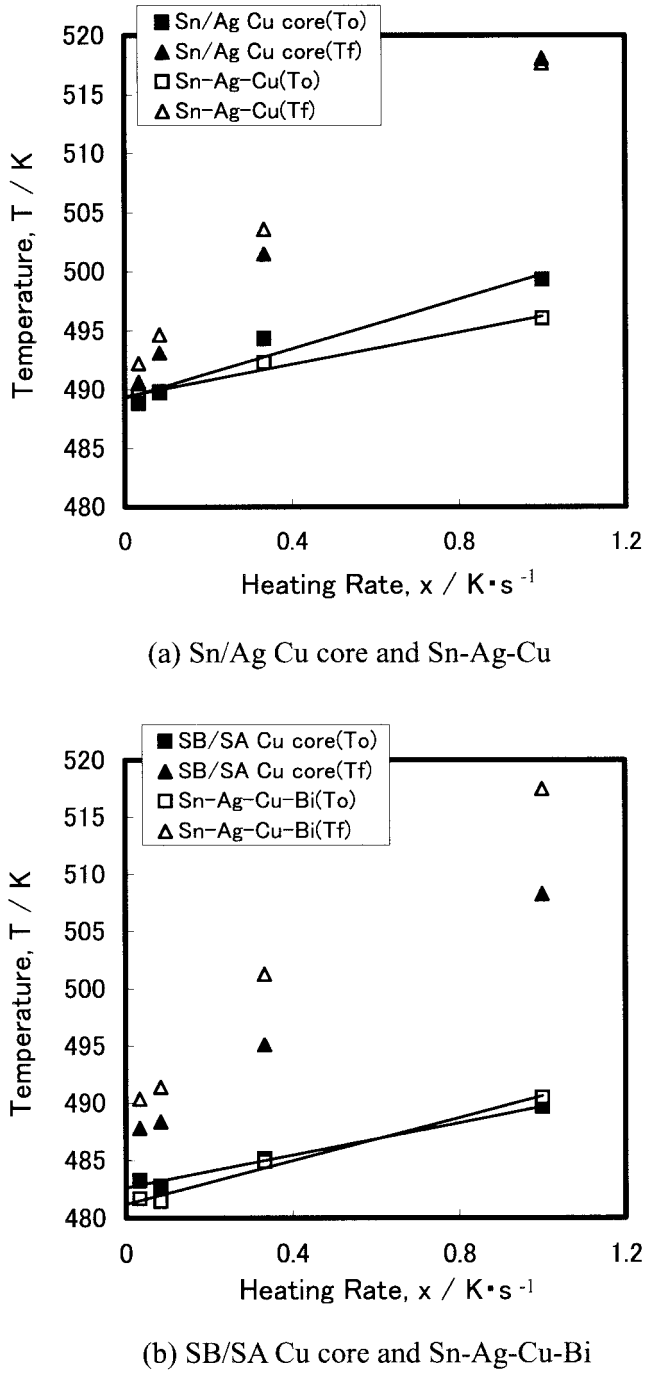

Fig. 4 Relationship between *To* and *Tf* for various solders and heating rate for (a) Sn/Ag Cu core, (b) Sn–Ag–Cu, (c) SB/SA Cu core and (d) Sn–Ag–Cu–Bi solder balls.

3.3 Joint microstructure of BGA joints

Figure 5 shows the microstructures adjacent to the joint interface between solder and plating after reflow and subsequent heating at 423 K for 500 h for the joint between Au/Ni electroplated pads and (a) Sn/Ag Cu core, (b) SB/SA Cu core, (c) Sn–Ag and (d) Sn–Ag–Cu balls.

After reflow soldering with Cu-core solder balls, as shown in Figs. 5(a) and (b), solders exhibited a microstructure in which Ag_3Sn and Cu_6Sn_5 phases were dispersed in β-Sn matrix. This microstructure is almost the same as that observed for the Sn–Ag–Cu or Sn–Ag–Cu–Bi solder balls shown in Fig. 5(d). Little precipitation of Bi was observed, and al-

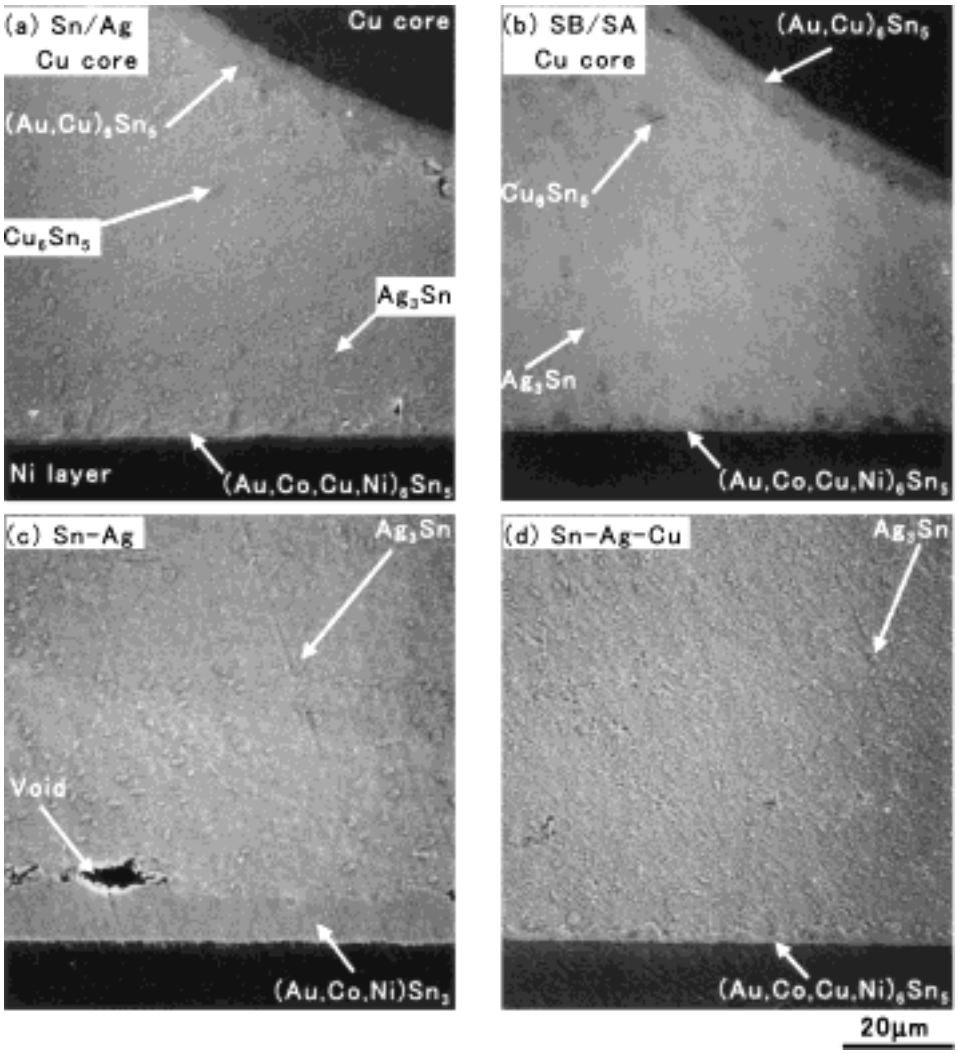

Fig. 5 Microstructures adjacent to the joint interface after reflow and subsequent heating at 423 K for 500 h for the BGA joint between Au/Ni electroplated pads and (a) Sn/Ag Cu core, (b) SB/SA Cu core, (c) Sn–Ag and (d) Sn–Ag–Cu balls.

most all of Bi was in solid form dissolved in Sn. After heat exposure at 423 K, Ag_3Sn changed morphology and assumed a more equiaxed shape.

The Au layer coated on the pad surfaces disappeared and dissolved into solders just after reflow, leaving the Ni layer exposed to the solder. We confirmed formation of a reaction layer at the interface between solders and the Ni layer for all the joints. Quantitative EDX analyses confirmed formation of Ni–Sn-based compounds for the joints using Sn–Ag solders. Changing the electroplated Au/Ni layer to an electrolysis-plated layer caused Ni–Sn compounds to change from $(Au, Co, Ni)Sn_3$ to Ni_3Sn_4 phase but left the Cu–Sn compound phase unchanged. Here, $(Au, Co, Ni)Sn_3$ phase does not correspond to any of the stable Ni–Sn compounds in the binary Ni–Sn phase diagram. However, Haimovich reported the formation of a metastable $NiSn_3$ phase on the boundary of Ni/Sn or Ni/Sn–Pb platings heat-treated at about 420 K.[16,17]

For the joints using Cu-containing or Cu-core solder balls, however, Cu- and Sn-based η'-$(Au, Cu, Ni)_6Sn_5$ reaction layers were formed. Changing from an electroplated coating to an electrolysis-plated coating did not change the phase. The authors previously reported that adding Cu to Sn–Pb or Sn–Ag solder changes the reaction layer formed at the interface with Ni plating from Ni–Sn based compounds to an η' phase.[7,8] For joints using Cu-core solder balls, Cu dissolved from the Cu-core ball during reflow affected the interaction with Ni plating. Similarly, an η'-$(Au, Cu)_6Sn_5$ reaction layer was formed on the boundary between the solder and the Cu core.

Figure 6 illustrates the changes in the thickness of the reaction layer formed by the interaction of solders with (a) electroplated and (b) electrolysis-plated Ni as a function of heat exposure time at 423 K. As evident from the figure, the $NiSn_3$ reaction layer formed between the Sn–Ag solder and the electroplated Ni grows much faster than any other reaction layer. The enhanced interfacial reaction between Sn and Ni introduced Kirkenndall voids at the solder-$NiSn_3$ interface as shown in Fig. 5(c). The growth rate of the η' reaction layer at the Cu/Sn interface is generally higher than that of the Ni_3Sn_4 reaction layer at the Ni–Sn interface.[18] This can be confirmed in this research if the growth rate of Ni_3Sn_4 formed for an Sn–Ag/electrolysis-plated Ni interface is compared with that of η'-Cu_6Sn_5 formed at the solder-Cu core interface in Fig. 6(b). However, the growth rate of η'-$(Au, Cu)_6Sn_5$ formed solder-Ni plating became comparable with that of Ni_3Sn_4 because

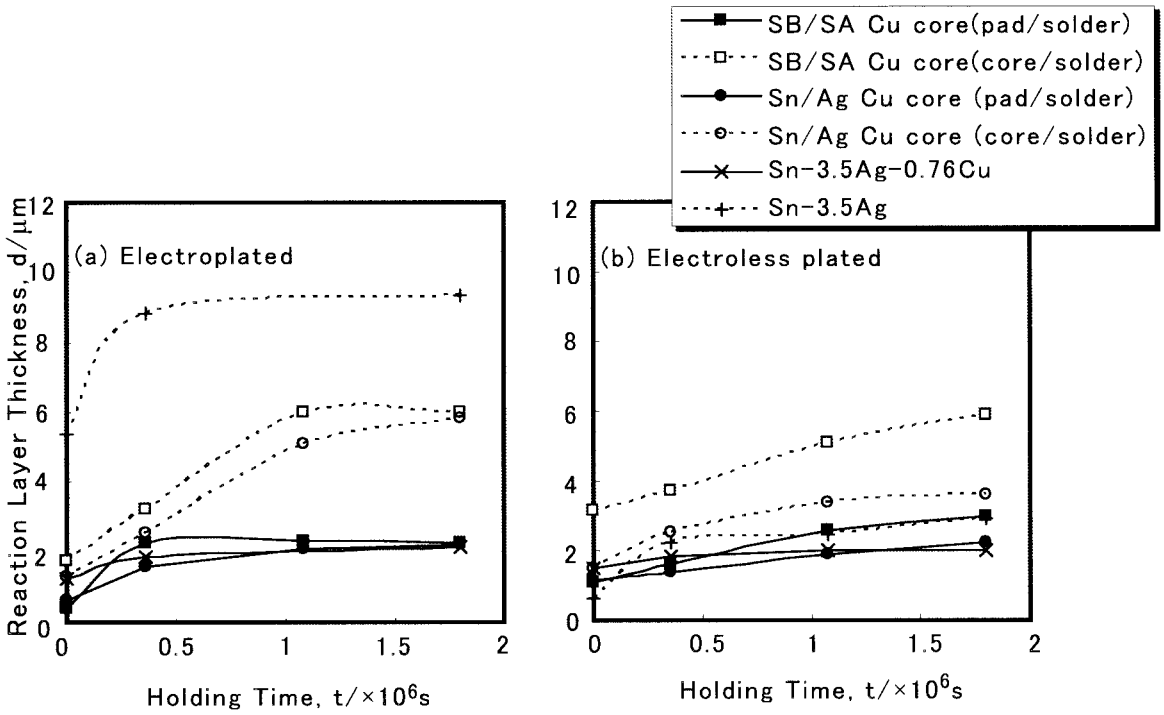

Fig. 6 Changes in the thickness of the reaction layer formed by the interaction of solders with (a) electro and (b) electroless Ni Plating as a function of heat exposure time at 423 K.

most of the Cu in the solder ball was exhausted in forming the η' reaction layer and hardly existed in the solder after reflow. Addition of Bi to solders hardly affected the formation and growth behavior of the reaction layer.

3.4 Shear strength of BGA joints

Figure 7 depicts the changes in shear fracture load of the BGA joints using Au/Ni (a) electroplated and (b) electrolysis-plated Cu pads as a function of heat exposure time at 423 K. The shear fracture load does not always correspond to the joint strength due to the different joint morphologies for each solder, but at least the changes of the load during high-temperature storage indicate the joint reliabilities.[19,20] All joints fractured at a lower shear load after heat exposure than did as-reflowed joints. However, joints using Cu-core solder balls exhibited shear strength comparable to that of previously alloyed solder balls.

Figure 8 schematically illustrates crack paths for the Cu-core solder-pad joint. Mode 1 indicates a fracture in the Cu_6Sn_5, and mode 2, a fracture along the pad-substrate interface. Table 3 shows the fracture mode defined in Fig. 8 during shear tests of the BGA joints using various solders. We confirmed that fractures occurred in the solders for reflowed joints or joints heat-treated for less than 100 h. We confirmed changes in fracture modes for the joints using Sn–Ag solders and for the joints of SB/SA or Sn–Ag–Bi–Cu solder and electrolysis-plated Ni. When a fracture occurs in the solders, the degradation of joint strength is attributed to the microstructural evolution of solders. This is related to the coarsening of the eutectic Sn–Ag_3Sn or Sn–Ag_3Sn–Cu_6Sn_5 structure resulting from the failure of the Ag_3Sn network structure for Sn–Ag based solders. Although the effect of adding Cu to solders is slight due to the small volume fraction of η', the

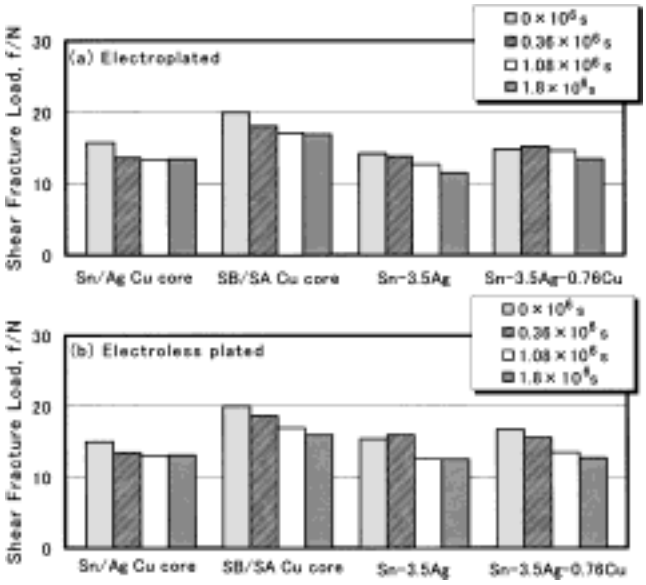

Fig. 7 Changes in shear fracture load of the BGA joints using Au/Ni (a) electroplated and (b)electroless plated Cu pads as a function of heat exposure time at 423 K.

effect of solid solution hardening of Sn by adding Bi is very significant. The change in fracture mode for the solder-pad interface due to heat exposure suggests decreased strength at the interface due to the enhanced interaction between solder and Ni. For the interfaces between Sn–Ag solders and electroplated Ni, the thickness of the reaction layer increases to about 10 μm, and Kirkendall voids were introduced, resulting in the degradation of joint strength. Although the Ni_3Sn_4 reaction layer grows very little for the joints of Sn–Ag solder with electrolysis-plated Ni, we confirmed formation of a P-

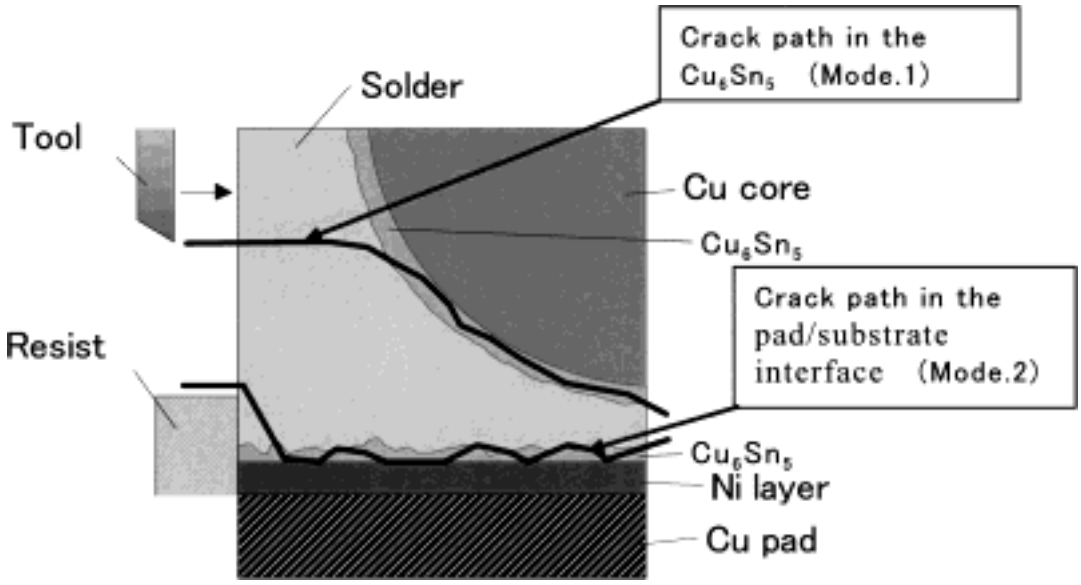

Fig. 8 Schematic illustration of crack paths showing shear test for BGA joints. Mode 1 referes to fractures in the Cu_6Sn_5 reaction layer formed between Cu ball and solder. Mode 2 refers to fractures at the solder/Ni interface.

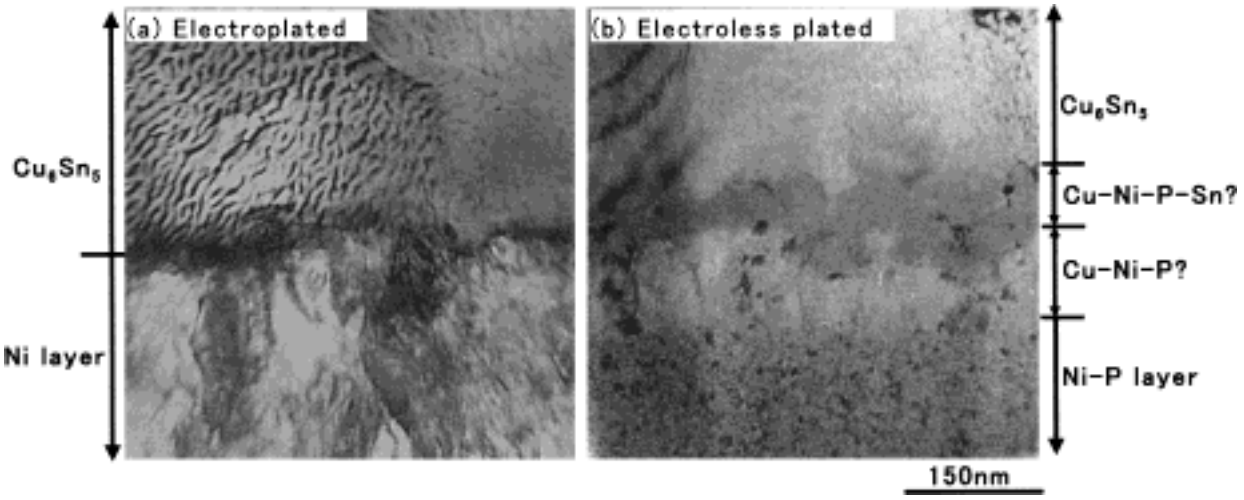

Fig. 9 Bright field TEM microstructure adjacent to the joint interface after reflow and subsequent heating at 423 K for 500 h for the BGA joint between SB/SA Cu core ball and Au/Ni (a) electroplated and (b) electroless plated Cu Pads.

Table 3 Fracture mode defined in Fig. 8 during shear test of the BGA joints.

		Solder balls				
		Sn/Ag Cu core	SB/SA Cu core	Sn–Ag	Sn–Ag–Cu	Sn–Ag–Cu–Bi
Plating	Electro	Mode 1	Mode 1	Mode 1 → Mode 2	Mode 1	Mode 1
	Electroless	Mode 1	Mode 1 → Mode 2	Mode 1 → Mode 2	Mode 1	Mode 1 → Mode 2

enriched Ni–P layer by SEM and TEM observations. The brittle Ni_3P-based layer degraded the joint strength, as expected from discussions of the effect of P-rich layer formation on the joint strength by many researchers.[21] While formation of a P-enriched layer has also been observed for joints using Sn–Ag–Cu solders, the layer is thinner than that for Sn–Ag solders and consequently has been considered to have little effect on joint strength.[22] In the present research, how-

ever, fractures began to occur at the joint interface for SB-SA joints due to thermal exposure. Figure 9 shows the bright field TEM microstructure adjacent to the joint interface after reflow and the subsequent heating at 423 K for 500 h for the BGA joint between the SB-SA Cu-core ball and Au/Ni (a) electroplated and (b) electrolysis-plated Cu pad Cu-core balls with electrolysis-plated Ni. As shown in Fig. 9(b), two reaction layers containing P formed, although a detailed compositional and crystallographic analysis is still in progress. These two reaction layers were also observed at the joint between the Sn–Ag–Cu solder and the Ni–P electrolysis-plated layer. Since these layers are thinner than those of Sn–Ag solders, they hardly affect the joint strength for the joints using Sn–Ag–Cu solder. For the joints using Sn–Ag–Cu solders containing Bi, however, their effects become significant and fractures occur around them because of the increased strength of solders.

4. Conclusion

In this work, we fabricated Cu-core Sn–Ag solder balls by plating pure Sn and Ag onto Cu balls. We also fabricated Cu-core, multicomponent Sn–Ag–Bi balls by sequentially coating binary Sn–Ag and Sn–Bi solders onto Cu balls. We investigated the melting of the Sn/Ag or Sn–Bi/Sn–Ag (SB/SA) plating by differential scanning calorimetry. The solderability of the BGA joint with the Ni/Au coated Cu pad was also evaluated by observing the microstructure and performing joint shear tests for both the as reflowed and thermally exposed joints. We compared the results obtained with those using the previously alloyed commercial Sn–Ag, Sn–Ag–Cu and Sn–Ag–Cu–Bi balls. The main results from this research are described below.

(1) The Sn/Ag plating on Cu ball began to melt at a rather low temperature, the eutectic temperature of Sn–Ag–Cu. This was ascribed to the diffusion of Cu and Ag into the Sn plating during the heating process. Similarly, SB/SA balls also exhibited almost the same melting behavior as previously alloyed Sn–2Ag–0.75Cu–3Bi solder.

(2) After reflow soldering with Cu-core solder balls, we observed a eutectic microstructure composed of β-Sn, Ag_3Sn, and Cu_6Sn_5 phases in the solder, and the η'-$(Au, Cu, Ni)_6Sn_5$ reaction layer was formed at the interface between the solder and the Ni plating. The joint microstructure was almost the same as that obtained when using Sn–Ag–Cu or Sn–Ag–Cu–Bi solders since Cu dissolved from the Cu-core ball into solders during melting of solders.

(3) The growth rate of the η' reaction layer formed at the solder-Ni interface during heat exposure at 423 K was much lower than that for the $NiSn_3$ reaction layer. The suppression of reaction layer growth for the joints using solders containing Cu was attributed to Cu in the solder ball being mostly exhausted to form the η' reaction layer with little remaining in the solder after reflow. Moreover, the η' layer functioned as a barrier to suppress the rapid Ni–Sn interfacial reaction because each element should diffuse through this η' layer.

(4) Joints using Cu-core solder balls exhibited shear strength comparable to those using previously alloyed solder balls. The slower growth rate of the η'-$(Au, Cu, Ni)_6Sn_5$ reaction layer formed at the solder-plating interface prevented the degradation of joint strength during aging at 423 K. Joints using SB/SA Cu-core balls retained the highest shear fracture load.

(5) Two reaction layers containing P formed between the η'-$(Au, Cu, Ni)_6Sn_5$ reaction layer and the electrolysis-plated Ni for the joints using Cu-core solders or solders containing Cu. These layers were thinner than those of Sn–Ag solders and so hardly affected the joint strength for Sn–Ag–Cu solders. However, for the solders with Bi added and SB/SA balls, the effect became significant, resulting in fractures around these layers during shear tests.

REFERENCES

1) E. Bradley and K. Banerji: IEEE Trans. Comp. Pkg. & Mfg, Technol., **B18** (1996) 320–331.
2) M. Yamamoto: Jpn J. Electron. Mater, **9** (1997) 52–56 (Japanese).
3) S. Kiyono, K. Uenishi, K. F. Kobayashi, I. Shoji and M. Yamamoto: Jpn J. Electronics Packaging, **2** (1999) 298–302 (Japanese).
4) S. Kiyono, K. Uenishi. K. F. Kobayashi, I. Shoji and M. Yamamoto: Proc. 5th Sympo. on Microjoining and Assembly Technologies for Electronics, Yokohama Japan, (1999) 115–120 (Japanese).
5) T. Saeki, S. Kiyono, K. Uenishi, K. F. Kobayashi, I. Shoji and M. Yamamoto: Jpn J. Electronics Packaging, **4** (2001) 306–311 (Japanese).
6) S. Kiyono, T. Saeki, K. Uenishi. K. F. Kobayashi, I. Shoji and M. Yamamoto: Proc. 6th Sympo. on Microjoining and Assembly Technologies for Electronics, Yokohama Japan (2000) 125–130 (Japanese).
7) K. Uenishi, T. Saeki, Y. Kohara, K. F. Kobayashi, I. Shoji, M. Nishiura and M. Yamamoto: Mater. Trans. **42** (2001) 756–760.
8) K. Uenishi, Y. Kohara, S. Sakatani and K. F. Kobayashi: Proc. of 11th Sympo. on Microelectronics (MES2001), Osaka Japan, (2001) pp. 71–74 (Japanese).
9) Y. Kohara, T. Saeki, K. Uenishi, K. F. Kobayashi, I. Shoji and M. Yamamoto: Jpn J. Electronics Packaging, **4** (2001) 192–199 (Japanese).
10) S. K. Kang, R. S. Rai and S. Purushothaman: J. Electron. Mater. **25** (1996) 1113–1120.
11) A. Hirose, T. Fujii, T. Imamura and K. F. Kobayashi: Mater. Trans., **42** (2001) 794–802.
12) D. Mitlin, C. H. Raeder and R. W. Messler, Jr: Metall. Trans., **30A** (1999) 115–122.
13) Y. Kohara, T. Saeki, K. Uenishi, K. F. Kobayashi and M. Yamamoto: Proc. 7th Sympo. on Microjoining and Assembly Technologies for Electronics, Yokohama Japan, (2001) 119–124 (Japanese).
14) S. Sakatani, T. Saeki, Y. Kohara, K. Uenishi, K. F. Kobayashi and M. Yamamoto: Proc. of 11th Sympo. on Microelectronics (MES2001), Osaka Japan, (2001) 39–42 (Japanese).
15) S. Sakatani, Y. Kohara, K. Uenishi, K. F. Kobayashi and M. Yamamoto: Proc. 8th Sympo. on Microjoining and Assembly Technologies for Electronics, Yokohama Japan, (2002) 147–152.
16) J. Haimovich: Welding J., **68** (1989) 102s–111s.
17) J. Haimovich: Proc. AESF Annual Technical Conf., (1990) 689–712.
18) P. Kay and C. A. Mackay: Trans. Inst. Met. Fin., **57** (1979) 169–176.
19) M. Nishiura, K. Uenishi, T. Saeki, Y. Kohara and K. F. Kobayashi: submitted to Mater. Trans.
20) K. Uenishi, T. Saeki, Y. Kohara, M. Nishiura and K. F. Kobayashi: Proc. Fourth Pacific Rim Int. Conf. on Advanced Materials and Processing (PRICM4), (The Japan Institute of Metals, 2001) 1063–1066.
21) M. Ito, M. Yoshikawa, K. Okuno, M. Katagiri, T. Hiramori, A. Hirose and K. F. Kobayashi: Proc. 8th Sympo. on Microjoining and Assembly Technologies for Electronics, Yokohama Japan, (2002) 231–236 (Japanese).
22) M. Nishiura, A. Nakayama, S. Sakatani, Y. Kohara, T. Saeki, K. Uenishi and K. F. Kobayashi: Proc. of 7th International Conference on Today and Tommorow in Science and Technology of Welding and Joining (7WS), Kobe Japan, (2001) 1305–1310.